

Optomechanically induced transparency in Four-wave mixing atomic ensemble assisted Laguerre-Gaussian vortex cavity system

Yue-Tong Hao¹ and Yi-Mou Liu^{1,*}

¹Center for Quantum Sciences and School of Physics, Northeast Normal University, Changchun 130024, P. R. China.

(Dated: February 18, 2025)

We investigate the steady-state optical response of a Laguerre-Gaussian vortex cavity system integrated with cold atoms featuring a double- Λ energy level structure. Within this hybrid system, the atoms are driven by cavity mode and three coherent vortex beams, each carrying independent orbital angular momentum (OAM). We first check the steady-state output spectrum of the hybrid system in the passive/active case (without/with external cavity driving). Our findings reveal that the optomechanically induced transparency (OMIT) spectrum is modulated by the OAM difference ($\Delta\ell\hbar$) from the atomic component throughout the four-wave mixing (FWM) process. The resulting loop phase ($\Delta\ell\theta$) can achieve a switching effect on the absorption and gain behavior of the hybrid system for the probe beam. Additionally, the group delay, indicative of fast/slow light phenomena, is also tuned by $\Delta\ell$. We further display how the atomic OAM modulates the periodicity of the output spot pattern in the hybrid system. This research provides valuable insights into the modulation of optical responses in Laguerre-Gaussian vortex cavity systems.

I. INTRODUCTION

Unlike conventional Gaussian beams, vortex beams characterized by a phase factor $e^{i\ell\theta}$ carry the orbital angular momentum of $\ell\hbar$. Here, θ represents the azimuthal angle, and ℓ is the integer winding number of the vortex, which can take any integer value [1, 2]. OAM-carrying beams can be generated using various techniques, such as spatial light modulators (SLMs) [3–5], spiral phase plates (SPP) [6, 7], Q-plate [8], meta-Q-plate [9], and liquid-crystal Damman vortex grating [10]. When interacting with the matter, their specific properties give rise to a variety of interesting phenomena, including vortex slow light [11, 12], the entanglement of photons in OAM states [13], transfer of optical vortices [14–22], light-induced torque [23, 24], storage and retrieval of OAM-carrying beams [25, 26], and spatially dependent electromagnetically induced transparency (EIT) [27–29]. These approaches offer significant advantages in terms of all-optical control and reconfigurability. In addition, vortex beams are of interest in optical tweezers [30, 31], imaging and microscopy [32–34], sensing technologies for detecting molecules and nanostructures [35, 36], and optical communications [37–40].

Analogous to EIT [41], optomechanically induced transparency (OMIT) occurs when probe field photons interfere with up-converted sideband photons from the pump field via anti-Stokes processes, creating a transparency window in the resonance region. This concept was theoretically proposed by G. S. Agarwal and Huang and experimentally demonstrated by Weis *et al.* in 2010 [42, 43]. As an important optical phenomenon in optomechanical systems, it has been applied to many fields, such as fast and slow light [44–47], optical storage [48–50], and optical switch [51, 52]. In 2007, Bhattacharya *et al.* proposed a Laguerre Gaussian (L-G) cavity with Laguerre Gaussian modes [53]. Distinct from the Fabry-Perot (F-P) cavity, it can use the rotational degrees of freedom to couple the optical field and exchange OAM with a

spiral phase element. This provides a promising platform for multimode macroscopic quantum phenomena. Currently, investigations into the L-G cavity encompass a range of topics, including quantum entanglement [54–57], mechanical cooling [58], and OMIT [59–62]. The application of OMIT in L-G cavity system provides new tools for parameter measurement, including OAM. While OAM adds a new modulation parameter to the optomechanical system, its effect on the steady-state optomechanical response is limited. This influence is mainly seen in the unchanged rotation-optical coupling strength $g_\phi = c\ell/L$, which remains constant after preparation in L-G cavities. In general cavity optomechanical systems, the easily encoded OAM information is lost during the modulus operation, resulting in both a waste of quantum resources and a limitation on potential applications. Therefore, effectively harnessing the modulation effect of OAM in L-G cavity systems is a key issue that warrants further exploration.

In this paper, we place a double- Λ type four-level atomic ensemble in a L-G cavity. Utilizing four-wave mixing processes (FWM), we try to propose a scheme to transfer orbital angular momentum from the coherent laser beams (driving atoms) to the cavity mode, with the goal of modulating the system's optical response using OAM. By examining two distinct FWM coupling cases, we find that the loop OAM, denoted as $\Delta\ell\hbar$, from the atomic ensemble can switch the system's output properties between absorption ($\Delta\ell = 0$) and gain ($\Delta\ell = 2$) with $\theta = \pi/2$. This OAM-induced switch also directly influences the group delay features of the output beam, modulating both slow and fast light conditions. Further, it is explored how the output spot pattern is affected by varying the detuning between the driving frequency, the cavity mode frequency, and the probe frequency, revealing the relationship between the periodicity of the spot petals and these parameters.

This work is organized through the following: Sec. II, where we describe the background model, and Sec. III, where we discuss the steady-state optical response of the hybrid system, including OMIT spectra, conversion of fast/slow light, and optical vortices in the output field. We summarize, at last,

* liuym605@nenu.edu.cn

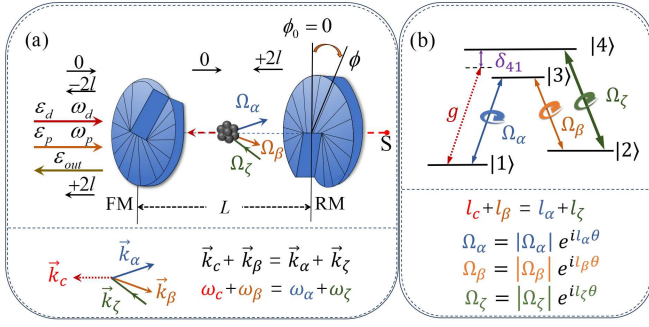


FIG. 1. Schematic diagram of the system: (a) An optomechanical cavity with a rigidly fixed mirror (FM) and a rotational one (RM), the cavity mode is the L-G mode. The equilibrium position of the rotational mirror is ϕ_0 . Inside the cavity, a double- Λ four-level type atomic ensemble is driven by three coherent laser fields, and the energy level structure is shown in panel (b). The directions of the three driving fields are shown at the bottom of panel (a), and their wave vectors satisfy $\vec{k}_c + \vec{k}_\beta = \vec{k}_\alpha + \vec{k}_\zeta$. The topological charge on the vortex beams (OAM) has been indicated.

our conclusions in Sec. IV.

II. MODEL AND EQUATIONS

A Laguerre-Gaussian cavity consists of two spiral phase elements: one is fixed in place, while the other is mounted on a support structure, labeled as S , which enables it to rotate around the cavity axis. The fixed mirror, labeled FM in Fig. 1(a), has an inversion-symmetric structure, which ensures that any beam transmitted through it retains its topological charge, while a beam reflected from FM loses a charge of $2l$. The rear rotating mirror (RM), which is perfectly reflective, adds a topological charge of $2l$ to the reflected beam. Consequently, within the L-G cavity, the orbital angular momentum of the beam propagating to the right is always 0, while that of the beam moving to the left is consistently $2l\hbar$, under the normal Gaussian mode driving.

As illustrated in Fig. 1(a), the L-G cavity is driven by a normal Gaussian pump field (frequency ω_d), and it is probed by a weak field with frequency ω_p . Inside the L-G cavity, there is a double- Λ type four-level atomic ensemble, consisting of two ground states $|1\rangle$ and $|2\rangle$ and two excited states $|3\rangle$ and $|4\rangle$, as depicted in Fig. 1(b). The transition $|1\rangle \leftrightarrow |4\rangle$ is probed by the quantum cavity mode with coupling strength $g = \wp_{14} \sqrt{\omega_c / (2\hbar\epsilon_0 V)}$, where ϵ_0 (V , \wp_{14}) is the permittivity of free space (the cavity mode volume, the transition dipole moment). Meanwhile, the transitions $|1\rangle \leftrightarrow |3\rangle$, $|2\rangle \leftrightarrow |3\rangle$, and $|2\rangle \leftrightarrow |4\rangle$ are driven by classical coherent fields with half Rabi frequencies $\Omega_\mu = \wp_\nu E_\mu / 2\hbar$ ($\mu \in \{\alpha, \beta, \zeta\}$ and $\nu \in \{13, 23, 24\}$), corresponding to the respective frequencies $\omega_{\alpha, \beta, \zeta}$.

The Hamiltonian of the system takes the form $H = H_0 +$

$H_{af} + H_{om}$, with

$$\begin{aligned}
 H_0 &= \hbar \sum_{k=1}^N \sum_{q=1}^4 \omega_q \sigma_{qq}^{(k)} + \hbar \omega_c a^\dagger a + \frac{L_z^2}{2I} + \frac{1}{2} I \omega_\phi^2 \phi^2, \\
 H_{af} &= -\hbar \sum_{k=1}^N [g a \sigma_{41}^{(k)} + \Omega_\alpha \sigma_{31}^{(k)} e^{-i\omega_\alpha t} \\
 &\quad + \Omega_\beta \sigma_{32}^{(k)} e^{-i\omega_\beta t} + \Omega_\zeta \sigma_{42}^{(k)} e^{-i\omega_\zeta t}] + h.c., \\
 H_{om} &= -\hbar g_\phi a^\dagger a \phi + i\hbar (\mathcal{E}_d a^\dagger e^{-i\omega_d t} + \mathcal{E}_p a^\dagger e^{-i\omega_p t}) + h.c..
 \end{aligned} \tag{1}$$

Here H_0 represents the free Hamiltonian including atomic ensemble with frequencies ω_q ($q \in \{1, 2, 3, 4\}$ and $\omega_1 = 0$), the cavity mode (frequency ω_c) and the RM mirror (frequency ω_ϕ). $\sigma_{pq}^{(k)} = |p\rangle_{kk}\langle q|$ is defined as the projection ($p = q$) or transition ($p \neq q$) operator of the k th atom; a (a^\dagger) denotes the annihilation (creation) operator of the cavity field; $I = MR^2/2$ gives the moment of inertia of the RM mirror about the cavity axis, where M and R are the mass and radius of the mirror, respectively; L_z (ω_ϕ , ϕ) is the angular momentum (the angular rotation frequency, the angular displacement) with satisfying the commutation relation $[L_z, \phi] = -i\hbar\delta$. And therefore, H_{af} reads the atom-field and atom-cavity interactions. H_{om} contains the optomechanical interaction with the coupling strength $g_\phi = cl/L$ (c the vacuum speed of light, l the OAM quantum number of cavity mode, L the cavity length) and those between the cavity and the two external fields with amplitudes $\mathcal{E}_{d,p} = \sqrt{2P_{d,p}\kappa/\hbar\omega_{d,p}}$, where P_d (P_p) is the power of the driving (probe) field.

With low excitation and large number approximation of atomic ensemble, the dynamics of the system can be described by the following Heisenberg-Langevin equations:

$$\begin{aligned}
 \dot{\phi} &= L_z/I, \\
 \dot{L}_z &= -\gamma_\phi L_z - I\omega_\phi^2 \phi + \hbar g_\phi a^\dagger a - \sqrt{2\gamma_\phi} \xi(t), \\
 \dot{a} &= -[\kappa + i\omega_c - ig_\phi \phi]a + ig' \varrho_{14} + \mathcal{E}_d e^{-i\omega_d t} \\
 &\quad + \mathcal{E}_p e^{-i\omega_p t} + \sqrt{2\kappa} a^{in}(t), \\
 \dot{\varrho}_{14} &= -[\gamma_{14} + i\omega_4] \varrho_{14} + ig' a (\varrho_{11} - \varrho_{44}) \\
 &\quad + i\Omega_\zeta e^{-i\omega_\zeta t} \varrho_{12} - i\Omega_\alpha e^{-i\omega_\alpha t} \varrho_{34} + \sqrt{2\gamma_{14}} f_{14}(t),
 \end{aligned} \tag{2}$$

where $g' = g\sqrt{N}$ with N denoting the atomic number density. Here we define the average projection or transition operator $\varrho_{pq} = \sum_{k=1}^N \sigma_{pq}^{(k)} / \sqrt{N}$ for convenience. In addition, we phenomenologically add the mirror damping rate (the cavity decay rate, the atomic dephasing rates) as γ_ϕ (κ , γ_{pq}); and the term ξ (a^{in} , f_{pq}) is also introduced to represent the quantum fluctuations of the rotating mirror (the cavity field, and the external field driving the atoms).

We performed the following frame rotation of the above equations: $a = a e^{-i\omega_d t}$, $\varrho_{14} = \varrho_{14} e^{-i\omega_d t}$, $\varrho_{13} = \varrho_{13} e^{-i\omega_\alpha t}$, $\varrho_{23} = \varrho_{23} e^{-i\omega_\beta t}$, $\varrho_{24} = \varrho_{24} e^{-i\omega_\zeta t}$, $\varrho_{12} = \varrho_{12} e^{-i(\omega_d - \omega_\zeta)t}$,

$\varrho_{34} = \varrho_{34} e^{-i(\omega_d - \omega_\alpha)t}$, which yields

$$\begin{aligned} \dot{a} &= -[\kappa + i\Delta_c - ig_\phi\phi]a + ig'\varrho_{14} + \mathcal{E}_d + \mathcal{E}_p e^{-i\delta_p t} \\ &\quad + \sqrt{2\kappa}a^{in}(t), \\ \dot{\varrho}_{14} &= -(\gamma_{14} + i\delta_c)\varrho_{14} + ig'a(\varrho_{11} - \varrho_{44}) + i\Omega_\zeta\varrho_{12} \\ &\quad - i\Omega_\alpha\varrho_{34} + \sqrt{2\gamma_{14}}f_{14}(t), \end{aligned} \quad (3)$$

where $\Delta_c = \omega_c - \omega_d$ (denoting the detuning between the cavity mode and the driving field), $\delta_c = \omega_4 - \omega_c$ (denoting the detuning between the cavity mode and the corresponding energy level of the atom), $\delta_{31} = \omega_3 - \omega_\alpha$, $\delta_{21} = \delta_c - \delta_{42} = \omega_2 - \omega_d + \omega_\zeta$. Assuming all the fields couple to the atomic ensemble resonantly, we have $\delta_{31} = \delta_{32} = \delta_{42} = 0$.

Considering the quantum fluctuations of each operator $O \in \{\phi, L_z, a\}$ in the steady state, we linearize around the steady-state value O_s by adding the fluctuation operator δO , such that $O = O_s + \delta O$. Then we can obtain the following steady-state solutions

$$\begin{aligned} \phi_s &= \frac{\hbar g_\phi |a_s|^2}{I\omega_\phi^2}, \\ a_s &= \frac{\mathcal{E}_d + ig'B_f}{\kappa + g'\text{Im}[A_f] + i(\bar{\Delta} - g'\text{Re}[A_f])}, \\ \varrho_{14}^s &= A_f a_s + B_f, (f = 0, 1) \end{aligned} \quad (4)$$

where $\bar{\Delta} = \Delta_c - g_{\phi_s}\phi_s$ denotes the effective detuning between the cavity field modes and the driving field when the rotating mirror deviates from its equilibrium position. Equation (4) shows that the FWM atoms introduce two effects to the system: first, the cavity decay rate increases by $g'\text{Im}[A_f]$; second, the cavity frequency is effectively shifted by $g'\text{Re}[A_f]$. It is worth noting that ϱ_{14}^s contains two terms, the first of which represents a linear term $A_f a_s$ and the second a four-wave mixing term B_f . In this study, two conditions are considered: one in which Ω_α is a weak field with

$$\begin{aligned} A_0 &= \frac{g'(\delta_c\gamma_e - i|\Omega_\beta|^2)}{\delta_c^2\gamma_e - (|\Omega_\beta|^2 + |\Omega_\zeta|^2)\gamma_e - i\delta_c(|\Omega_\beta|^2 + \gamma_e^2)}, \\ B_0 &= \frac{i\Omega_\alpha\Omega_\beta^*\Omega_\zeta}{\delta_c^2\gamma_e - (|\Omega_\beta|^2 + |\Omega_\zeta|^2)\gamma_e - i\delta_c(|\Omega_\beta|^2 + \gamma_e^2)}, \end{aligned} \quad (5)$$

and the other in which Ω_β is a weak field ($\Omega_\alpha = \Omega_\zeta = \Omega$) with

$$\begin{aligned} A_1 &= \frac{-g'\delta_c\gamma_e(\gamma_e^2 - |\Omega|^2 + i\delta_c\gamma_e/2)}{(i\delta_c + \gamma_e)(4|\Omega|^2 - \delta_c^2 + 2i\delta_c\gamma_e)(2|\Omega|^2 + \gamma_e^2)}, \\ B_1 &= \frac{\Omega^2\Omega_\beta^*\gamma_e(\delta_c - 2i\gamma_e)}{(i\delta_c + \gamma_e)(4|\Omega|^2 - \delta_c^2 + 2i\delta_c\gamma_e)(2|\Omega|^2 + \gamma_e^2)}. \end{aligned} \quad (6)$$

To further investigate the vortex light specific to the L-G cavity, we made the three coherent fields incident on the atomic ensemble are L-G beams carrying different OAM ($\ell_\mu\hbar$). In this case, the Rabi frequency of the three fields is characterized as

$$\Omega_\alpha = |\Omega_\alpha|e^{i\ell_\alpha\theta}, \Omega_\beta = |\Omega_\beta|e^{i\ell_\beta\theta}, \Omega_\zeta = |\Omega_\zeta|e^{i\ell_\zeta\theta}, \quad (7)$$

where θ is the azimuthal angle. For a L-G light beam, we may write

$$|\Omega_\mu| = \mathcal{E}_\mu \left(\frac{r}{w}\right)^{|\ell|} e^{-\frac{r^2}{w^2}}, (\mu = \alpha, \beta, \zeta) \quad (8)$$

where r represents the distance from the vortex core, w represents the beam waist, and \mathcal{E}_μ is the strength of the vortex beam. Substituting the above transformation into Eq. (4), the expression for steady state-solutions only changes for B . Then we define the change as \tilde{B} , with $\tilde{B} = B \cdot e^{i\Delta\ell\theta}$ and $\Delta\ell = \ell_\alpha - \ell_\beta + \ell_\zeta$. In general, the mean value of each dynamic variable considered here is much larger than its fluctuation, i.e. $|O_s| \gg \delta O$. In this condition, one can safely neglect the nonlinear terms, e.g. $\delta a\delta a^\dagger$. Similarly, we can get the following linearized quantum Langevin equations:

$$\begin{aligned} \delta\dot{\phi} &= \delta L_z/I, \\ \delta\dot{L}_z &= -I\omega_\phi^2\delta\phi + \hbar g_\phi(a_s^*\delta a + a_s\delta a^\dagger) - \gamma_\phi\delta L_z, \\ \delta\dot{a} &= -(\kappa + i\Delta_c)\delta a + ig_\phi(\phi_s\delta a + a_s\delta\phi) + ig'\delta\rho_{14} \\ &\quad + \mathcal{E}_p e^{-i\delta_p t}, \\ \delta\dot{\varrho}_{14} &= A_f\delta a + \tilde{B}_f. \end{aligned} \quad (9)$$

For simplicity, we express the fluctuation operator in the following form:

$$\begin{aligned} \delta a &= \delta a_+ \mathcal{E}_p e^{-i\delta_p t} + \delta a_- \mathcal{E}_p^* e^{i\delta_p t}, \\ \delta\phi &= \delta\phi_+ \mathcal{E}_p e^{-i\delta_p t} + \delta\phi_- \mathcal{E}_p^* e^{i\delta_p t}, \\ \delta L_z &= \delta L_{z+} \mathcal{E}_p e^{-i\delta_p t} + \delta L_{z-} \mathcal{E}_p^* e^{i\delta_p t}, \\ \delta\varrho_{14} &= \delta\varrho_{14+} \mathcal{E}_p e^{-i\delta_p t} + \delta\varrho_{14-} \mathcal{E}_p^* e^{i\delta_p t} \\ &= [A_f\delta a_+ + \tilde{B}_f] \mathcal{E}_p e^{-i\delta_p t} + [A_f^*\delta a_- + \tilde{B}_f^*] \mathcal{E}_p^* e^{i\delta_p t}. \end{aligned} \quad (10)$$

Substituting the above transformations into Eq. (9) yields

$$\begin{aligned}\delta a_+ &= \frac{\hbar g' \tilde{B}_f g_\phi^2 |a_s|^2 + (1 + i g' \tilde{B}_f)(Y^\dagger W + i g' A_f W + i \hbar g_\phi^2 |a_s|^2)}{XY^\dagger W - i(g' A_f W + \hbar g_\phi^2 |a_s|^2)(Y^\dagger - X) + 2\hbar g' g_\phi^2 A_f |a_s|^2 + g'^2 A_f^2 W}, \\ \delta a_- &= \frac{i \hbar g_\phi^2 |a_s|^2 W^\dagger + i g' \tilde{B}_f^\dagger W^\dagger (X^\dagger W^\dagger + i g' A_f^\dagger W^\dagger)}{X^\dagger Y W^\dagger + i(g' A_f^\dagger W^\dagger + \hbar g_\phi^2 |a_s|^2)(Y - X^\dagger) + 2\hbar g' g_\phi^2 A_f^\dagger |a_s|^2 + g'^2 A_f^{\dagger 2} W^\dagger},\end{aligned}\quad (11)$$

where $W = I(\omega_\phi^2 - \delta_p^2 - i\gamma_\phi \delta_p)$, $X = \kappa + i(\Delta_c - \delta_p - g_\phi \phi_s)$, and $Y = \kappa + i(\Delta_c + \delta_p - g_\phi \phi_s)$.

III. STEADY-STATE OPTICAL RESPONSE OF THE OUTPUT FIELD

In this section, we focus on the steady-state optical response, including absorptive and dispersive characteristics, of the output field. We also investigate the correlation between these characteristics and the orbital angular momentum imparted by the driving field of the cavity mode and the coupled atoms, as well as the coupling strength of the cavity field. The parameters employed are sourced from the referenced studies [53, 54], including the cavity length $L = 0.2$ mm, the wavelength of the driving field $\lambda = 810$ nm, the cavity radius $R = 10$ μm , the cavity mass $M = 100$ ng, the mirror's angular frequency $\omega_\phi = 2\pi \times 35$ MHz, the mirror's decay rate $\gamma_\phi = 2\pi \times 140$ Hz, and the cavity's decay rate $\kappa = 2\pi \times 8$ MHz. The Rabi frequencies for the three laser beams are set at $\Omega_\alpha = 0.02 \times 2\pi$ MHz, $\Omega_\beta = 10 \times 2\pi$ MHz, and $\Omega_\zeta = 10 \times 2\pi$ MHz, respectively.

To examine the dynamic stability of the system, we further rewrite the Langevin equations by $\dot{u}(t) = Mu(t) + v(t) + \eta(t)$, which are expressed in terms of the quadrature operators $u(t) = (\delta\phi, \delta L_z, \delta U, \delta V)^T$ with $U = \frac{1}{\sqrt{2}}(\delta a + \delta a^\dagger)$ and $V = \frac{1}{\sqrt{2}i}(\delta a - \delta a^\dagger)$ being the amplitude and phase quadratures of the cavity field. We also set $v(t) = (0, 0, \frac{1}{\sqrt{2}}(\varepsilon_p e^{-i\delta_p t} + \varepsilon_p^* e^{i\delta_p t}) - \sqrt{2}g' \text{Im}[\tilde{B}_f], \frac{1}{\sqrt{2}i}(\varepsilon_p e^{-i\delta_p t} - \varepsilon_p^* e^{i\delta_p t}) + \sqrt{2}g' \text{Re}[\tilde{B}_f])^T$, and $\eta(t) = (0, \delta \varepsilon^{in}, \sqrt{2}\kappa \delta U^{in}, \sqrt{2}\kappa \delta V^{in})$ with $\delta U^{in} = \frac{1}{\sqrt{2}}(a_{in} + a_{in}^\dagger)$, $\delta V^{in} = \frac{1}{\sqrt{2}i}(a_{in} - a_{in}^\dagger)$ being the input vacuum noises and the evolution matrix

$$M = \begin{pmatrix} 0 & 1/I & 0 & 0 \\ -I\omega_\phi^2 & -\gamma_\phi & \sqrt{2}\hbar g_\phi a_r & \sqrt{2}\hbar g_\phi a_i \\ -\sqrt{2}g_\phi a_i & 0 & -\kappa' & \tilde{\Delta}_{A_f} \\ \sqrt{2}g_\phi a_r & 0 & -\tilde{\Delta}_{A_f} & -\kappa' \end{pmatrix}, \quad (12)$$

with $a_r = \frac{a_s + a_s^*}{2} = \text{Re}[a_s]$, $a_i = \frac{a_s - a_s^*}{2i} = \text{Im}[a_s]$ and $\tilde{\Delta}_{A_f} = \Delta_c - g' \text{Re}[A_f]$. Followed by the Routh-Hurwitz criterion [63], the real part of the eigenvalues of M should be strictly negative such that the system is stable, which gives

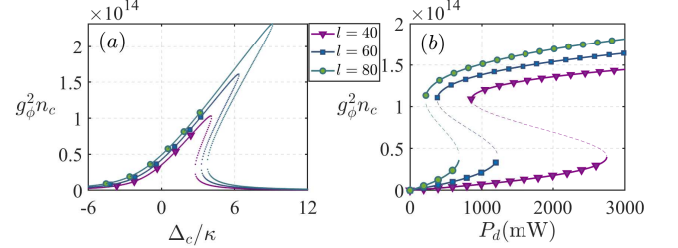


FIG. 2. The normalized cavity intensity $g_\phi^2 n_c$ (a) as a function of the dimensionless detuning Δ_c/κ for driving power $P_d = 200$ mW and (b) as a function of the driving power P_d for $\Delta_c/\kappa = 35$, with $l = 40$ (magenta-triangle), 60 (blue-square), 80 (olive-circle).

rise to the stability conditions below

$$\begin{aligned}s_1 &= (2\kappa' + \gamma_\phi)[\tilde{\Delta}_{A_f}^2 + \kappa'^2 + 2\gamma_\phi \kappa' + \omega_\phi^2] \\ &\quad - [\gamma_\phi \tilde{\Delta}_{A_f}^2 + \gamma_\phi \kappa'^2 + 2\kappa' \omega_\phi^2] > 0, \\ s_2 &= -2\hbar g_\phi^2 \tilde{\Delta}_{A_f} (a_r^2 + a_i^2) + I\omega_\phi^2 [\kappa'^2 + \tilde{\Delta}_{A_f}^2] > 0, \\ s_3 &= [\gamma_\phi I \tilde{\Delta}_{A_f}^2 + \gamma_\phi^2 I \kappa'^2 + 2I \kappa' \omega_\phi^2] s_1 - (2\kappa' + \gamma_\phi)^2 s_2 > 0.\end{aligned}\quad (13)$$

The investigation revealed that the range of parameters selected is consistent with the above inequality.

From Eq. (4), there is a higher-order equation for the average photon number, which predicts a possible multistability of the system and can be described by the following polynomial:

$$\begin{aligned}\frac{\hbar^2 g_\phi^4}{I^2 \omega_\phi^4} n_c^3 - \frac{2\hbar g_\phi^2 \tilde{\Delta}_{A_f}}{I \omega_\phi^2} n_c^2 + [\kappa'^2 + \tilde{\Delta}_{A_f}^2] n_c \\ = g'^2 |\tilde{B}_f|^2 - 2g' \mathcal{E}_d \text{Im}[\tilde{B}_f] + \mathcal{E}_d^2,\end{aligned}\quad (14)$$

which is a cubic equation about n_c and can be multistable. Fig. 2(a) examines the effective optomechanical coupling strength, given by $|G|^2 \propto g_\phi^2 n_c$, where $n_c = \langle a_s^\dagger a_s \rangle$ is the intracavity average photon number, across various detunings Δ_c between the cavity mode and the driving field. As anticipated, when l becomes sufficiently large ($g_\phi = cl/L$), this hybrid system exhibits multistability. With $\Delta_c = 30 \times 2\pi$ MHz, the multistable behavior is illustrated in Fig. 2(b) under different driving powers P_d . Eq. 14 further reveals that both Δ_c and l ($g_\phi = cl/L$) strongly influence the coefficient of n_c , while \mathcal{E}_d (or P_d) primarily controls the magnitude of the constant term, particularly with weak atom-cavity coupling $g' < \kappa$. Further, due to the weak nonlinearity ($\tilde{B}_f \ll g'$), the phase of OAM introduced by the atomic four-wave mixing process has a minimal effect on the stability of the system. Under the constraint

that the driving power is limited to $P_d < 230$ mW, we can safely analyze the optical response of the hybrid system in the single steady-state parameter range.

A. OMIT spectrum and fast/slow light conversion

We further check the steady optical response of the hybrid system. For simplicity, we will quantize the simple harmonic rotors (RM) as phonons, represented by creation (annihilation) operators b^\dagger (b),

$$\begin{aligned}\phi &= \sqrt{\frac{\hbar}{2I\omega_\phi}} (b^\dagger + b), \\ L_z &= i\sqrt{\frac{\hbar I\omega_\phi}{2}} (b^\dagger - b).\end{aligned}\quad (15)$$

Substituting the above transformations into Eq. (9) and (11) yields

$$\begin{aligned}\delta a_+ &= \frac{1 - ig'\tilde{B}_f}{[\kappa - i(\delta_p - g'A_f)] - G^2 a_s^\dagger a_s / (\gamma_\phi - i\delta_p)}, \\ \delta a_- &= \frac{-ig'\tilde{B}_f}{[\kappa + i(\delta_p + g'A_f)] - G^2 a_s^\dagger a_s / (\gamma_\phi + i\delta_p)},\end{aligned}\quad (16)$$

where defines $G a_s$ as effective optomechanical interaction rate with $G = g_\phi \sqrt{\hbar/2I\omega_\phi} = \frac{cl}{L} \sqrt{\hbar/2I\omega_\phi}$.

The output field of the cavity is defined as \mathcal{E}_{out} , using the standard input-output relation,

$$\mathcal{E}_{out} + \mathcal{E}_p e^{-i\delta_p t} + \mathcal{E}_d = 2\kappa a. \quad (17)$$

Expanding the output field as $\mathcal{E}_{out} = \mathcal{E}_{out}^s + \mathcal{E}_{out}^+ \mathcal{E}_p e^{-i\delta_p t} + \mathcal{E}_{out}^- \mathcal{E}_p e^{i\delta_p t}$, where \mathcal{E}_{out}^s denotes the steady-state form of the output field. Substituting it into Eq. (17), the output transmission spectrum can be obtained as

$$\begin{aligned}\mathcal{E}_{out}^s &= 2\kappa a_s - \mathcal{E}_d, \\ \mathcal{E}_{out}^+ &= 2\kappa \delta a_+ - 1, \\ \mathcal{E}_{out}^- &= 2\kappa \delta a_-.\end{aligned}\quad (18)$$

In order to study the response of the system to the probe field, the amplitude of the rescaled output to the probe field is

$$\mathcal{E}_T = \mathcal{E}_{out}^+ + 1 = 2\kappa \delta a_+ = u_p + iv_p, \quad (19)$$

where u_p and v_p represent the absorptive and dispersive coefficients of the optomechanical system, respectively. Moreover, the expression for the transmitted probe field is defined as $t_p = 1 - 2\kappa \delta a_+ = 1 - u_p - iv_p$.

Initially, it is discussed that the absorption spectrum $v_p(\omega)$ of the hybrid system in the absence of any extra-cavity driving field (*Passive case*), as depicted in Fig. 3(a₁) and (a₂). The light magenta-dotted curves and blue-dashed curves correspond to different weak-field coupling conditions for the atoms, namely $\Omega_\alpha/2\pi = 0.02$ MHz and $\Omega_\beta/2\pi = 0.02$ MHz, respectively. The olive-solid curves, on the other hand, represent those of the empty cavity for comparison (Lorentz-type

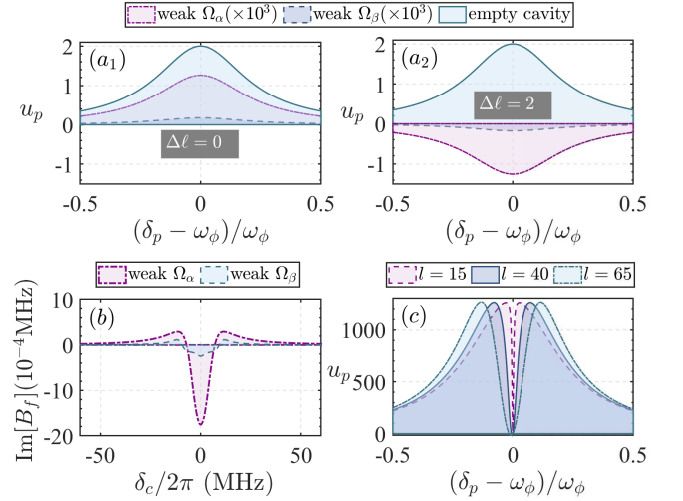


FIG. 3. The absorption curves as functions of the normalized optical detuning with (a₁) $\Delta l = 0$ and (a₂) $\Delta l = 2$ without cavity driving field ($P_d = 0$ mW) in conditions of weak field $\Omega_\alpha = 0.02$ MHz, weak field $\Omega_\beta = 0.02$ MHz, and empty cavity, respectively. Comparison of nonlinear effects at weak fields (b) for Ω_α and Ω_β , respectively. The absorption curves (c) as a function of the normalized optical detuning with different l in the case of $\Delta l = 0$. Other parameters take the values of $g' = 10^{-2}\gamma_e$, $P_d = 200$ mW.

curve). It is evident that the presence of atoms modifies the absorption spectrum of the hybrid system (Laguerre-Gaussian rotational-cavity), with the effective damping rate of the cavity $\kappa_{\text{eff}} = \kappa - \frac{g'^2 |\Omega_\beta|^2}{\gamma_e (|\Omega_\beta|^2 + |\Omega_\zeta|^2)}$ [A3]. Obviously, the phase information of the laser fields impinging on the atoms, influenced by OAM ($\varphi = \Delta l \cdot \theta$), produces distinct impacts on the absorption profile of the output field. This manifests as an absorption (gain) when $\Delta l = 0$ ($\Delta l = 2$), with $\varphi = \pi/2$. Moreover, the influence is more pronounced when Ω_α represents a weak field ($\Omega_\alpha \ll \Omega_\beta \simeq \Omega_\zeta$). With $\delta_c = 0$, we can obtain a stronger atomic nonlinear absorption $B_0 \simeq \frac{-i\Omega_\alpha}{2\gamma_e}$ than those ($B_1 \simeq \frac{-i\Omega_\beta^*}{2\gamma_e + \frac{4\Omega_\alpha^2}{\gamma_e}}$) for the case $\Omega_\beta \ll \Omega_\alpha \simeq \Omega_\zeta = \Omega$. It is also depicted in Fig. 3(b), under the assumption that both of the other two strong coherent coupling beams have a Rabi frequency of 10 MHz.

Figure 3(c) displays the absorptive coefficient as a function of normalized optical detuning $(\delta_p - \omega_\phi)/\omega_\phi$ for varying OAM values l of the cavity mode. Activation of the extra-cavity driving field ($E_d \neq 0$, *Active case*) results in a sharp decrease in the absorptive curve at the resonance frequency $\delta_p = \omega_\phi$, creating a transparent window, a signature of the OMIT effect [42, 43], similar to vibrating optomechanical systems. With an increase in OAM values l of the cavity mode, the OMIT window widens, and the optomechanical coupling constant $g_\phi = cl/L$ in the L-G cavity system correspondingly strengthens, resulting in the broadening of the OMIT window. In this case, the absorption coefficient reads $v_p \simeq \frac{2\kappa}{\kappa - i\delta_p - \frac{G^2 |a_s|^2}{\gamma_\phi - i\delta_p}}$ with effective optomechanical interac-

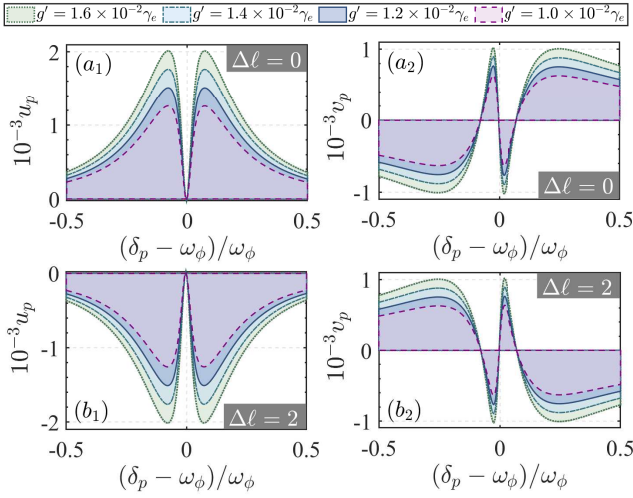


FIG. 4. The absorption curves (a₁) and dispersion curves (a₂) as a function of the normalized optical detuning with weak $\Omega_\alpha = 0.02$ MHz in the case of $\Delta\ell = 0$, $P_d = 200$ mW, and different coupling strength of the atomic and cavity fields: $g' = 0.01\gamma_e$, $g' = 0.05\gamma_e$, $g' = 0.1\gamma_e$ and $g' = 0.15\gamma_e$, respectively. Correspondingly, the case with weak $\Omega_\beta = 0.02$ MHz is shown in (b₁) and (b₂) with the same parameters.

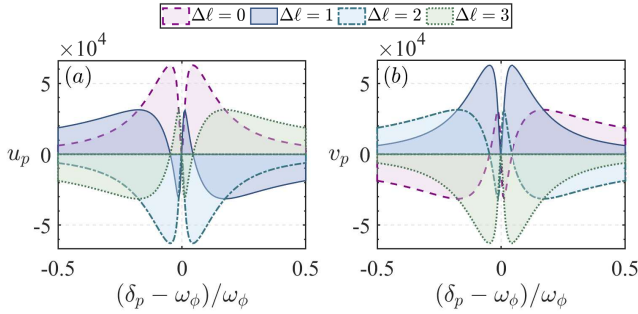


FIG. 5. The absorption curves (a) and dispersion curves (b) as a function of the normalized optical detuning $(\delta_p - \omega_\phi)/\omega_\phi$ with weak $\Omega_\alpha = 0.02$ MHz in the case of $\kappa = 2.85 \times 2\pi$ MHz, $g' = \gamma_e$, and different $\Delta\ell$: $\Delta\ell = 0, 1, 2$ and 3 . Other parameters are the same as Fig. 4.

$$\text{tion rate } Ga_s \quad (G = g_\phi \sqrt{\frac{\hbar}{2I\omega_\phi}} = \frac{cl}{L} \sqrt{\frac{\hbar}{2I\omega_\phi}}).$$

The impact of atomic-cavity coupling strength on the absorption and dispersion characteristics of the output field with $\Delta\ell = 0$ is depicted in Fig. 4(a₁) and (a₂), under the condition of a weak field Ω_α . With increasing coupling strength $g' = g\sqrt{N}$, the absorption window's peaks rise progressively, and the dispersion curve exhibits a pronounced steepness. In contrast to the $\Delta\ell = 0$ scenario, when $\Delta\ell = 2$, the system's output shows a trend of increasing optical gain ($v_p < 0$) and enhanced normal dispersion ($\frac{\partial u_p}{\partial \omega} > 0$) as the coupling strength augments, as illustrated in panels (b₁) and (b₂) of Fig. 4. From Eqs. (5), (16) and (19), the output of the hybrid

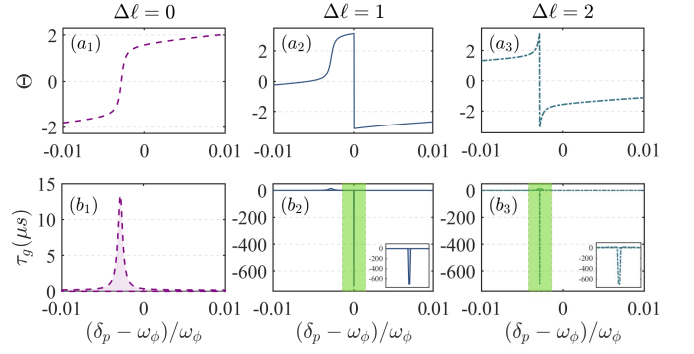


FIG. 6. The output phase and group delay curves under different $\Delta\ell$, are shown in panels (a₁)-(a₃) and panels (b₁)-(b₃), respectively. The subpanels correspond to the green range of panels (b₂) and (b₃). The other parameters are the same as in Fig. 4.

system reads

$$\mathcal{E}_T = \frac{2\kappa \left[1 - \frac{e^{i\Delta\ell\theta} g' \Omega_\alpha \Omega_\beta^2 \Omega_\zeta}{\gamma_e (\Omega_\beta^2 + |\Omega_\zeta|^2)} \right]}{\kappa_{\text{eff}} - i\delta_p - \frac{G^2 n_e}{\gamma_\phi - i\delta_p}}, \quad (20)$$

which predicts that different phase information ($\Delta\ell \cdot \theta$) leads to distinct absorption/gain (v_p) phenomena [A].

Fig. 5 demonstrates the possibility of engineering a unique symmetry relationship between the real and imaginary parts of the optical system in the frequency domain, under specific parameter settings [64–67]. These symmetries can be modulated by the atomic system introduced phase, which satisfies $\Delta\ell \cdot \theta = n\pi$, ($n = 0, 1, 2, \dots$). Establishing a correspondence between the system's frequency domain and spatial domain, as in [68], could enable the use of OAM within the system to achieve controllable parity-time symmetry (\mathcal{PT}) or parity-time antisymmetry (\mathcal{APT}) [69–72].

Furthermore, by altering the value of $\Delta\ell$, the transparency of the window and the slope of the dispersion curve will be adjustable, which also indicates that the system allows for fast and slow light conversion. The phase of the relevant output field at frequency ω_p (ω) can be written as

$$\Theta(\omega) = \arg[t_p(\omega)]. \quad (21)$$

Here, the rapid varying dispersion in the narrow transparency window may cause the group delay that can be expressed as [43, 73],

$$\tau_g = \frac{\partial \Theta}{\partial \omega}. \quad (22)$$

As the support, curves for the output field phase (the group delay for the system) versus relative probe frequency $(\delta_p - \omega_\phi)/\omega_\phi$ are displayed in Fig. 6 (a₁)-(a₃) [Fig. 6 (b₁)-(b₃)] with different $\Delta\ell$, near the resonant region. With null atomic OAM incidence ($\Delta\ell = 0$), the system exhibits normal dispersion, characterized by a consistently positive slope in phase or dispersion [see Fig. 6(a₁)]. Correspondingly, a time group delay peak around $(\delta_p - \omega_\phi)/\omega_\phi = -0.0028$ is observed, which corresponds to a slow light generation ($\tau_g = 14.0 \mu\text{s}$),

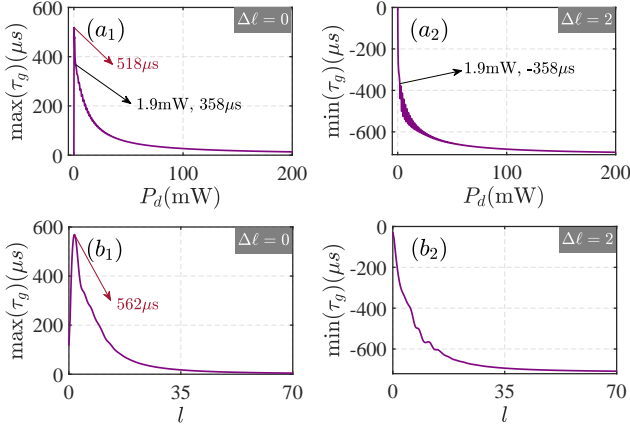


FIG. 7. Maximum transmission group delay $\tau_g^{(\max)}$ (a₁) and minimum negative group delay $\tau_g^{(\min)}$ (a₂) as a function of the driving field power P_d . Correspondingly, the maximum transmission group delay $\tau_g^{(\max)}$ (a₁) and minimum negative group delay $\tau_g^{(\min)}$ (a₂) as a function of l is shown in (b₁) and (b₂) with the same parameters. The rest of the parameters are the same as in Fig. 4.

as shown in Fig. 6(b₁). However, with $\Delta\ell = 1$ or 2, the phase dispersion changes rapidly (anomalous dispersion $\frac{\partial\theta}{\partial\omega} < 0$ appearing), which leads to large negative group velocity time delays (fast light appearing). It is noteworthy that the case with $\Delta\ell = 2$ generates fast light at the same frequency position ($\delta_p/\omega_\phi = 0.9972$) as the case with $\Delta\ell = 0$. The system group delay up to $-698 \mu\text{s}$, which is a considerable improvement over the previous work with the L-G cavity [74]. The proposed method readily facilitates the transition between fast and slow light propagation by merely altering the difference in orbital angular momentum, $\Delta\ell\hbar$, among the three classical coherence fields.

After the analysis of the effects of atomic nonlinearity, characterized by the expression $\vec{B}_f = B_f \cdot e^{i\Delta\ell\theta}$, on group delay, we proceed to investigate additional mechanisms for manipulating group delay. These include the optomechanical coupling constant, given by $g_\phi = \frac{cL}{L}$, and the driving intensity, expressed as $\mathcal{E}_d = \sqrt{\frac{2P_d\kappa}{\hbar\omega_d}}$. The maximum slow/fast light that can be produced by the system, under varying driving field powers [shown in Fig. 7 (a₁) and (a₂)] and different the vortex topological charge l induced by SPP [shown in Fig. 7 (b₁) and (b₂)]. In the scenarios with $l = 40$, the maximum group delay reaches $518 \mu\text{s}$ as the driving field power approaches zero, and the group delay decreases as the driving power further increases. What's more, the minimum negative group delay varies from $0 \mu\text{s}$ to $-698 \mu\text{s}$ as P_d varies within the range of $(0, 200)$ mW. With driving power $P_d = 1.9$ mW, a similar degree of reduction and increase in group velocity can be achieved by changing only $\Delta\ell$. When the driving power is 200 mW, the modulation of l on fast/slow light is similar to tuning the driving power P_d . The delay reaches a maximum of $562 \mu\text{s}$ as l approaches 0, and the minimum negative group delay gradually increases to $707 \mu\text{s}$ as l increases from 0 to 70.

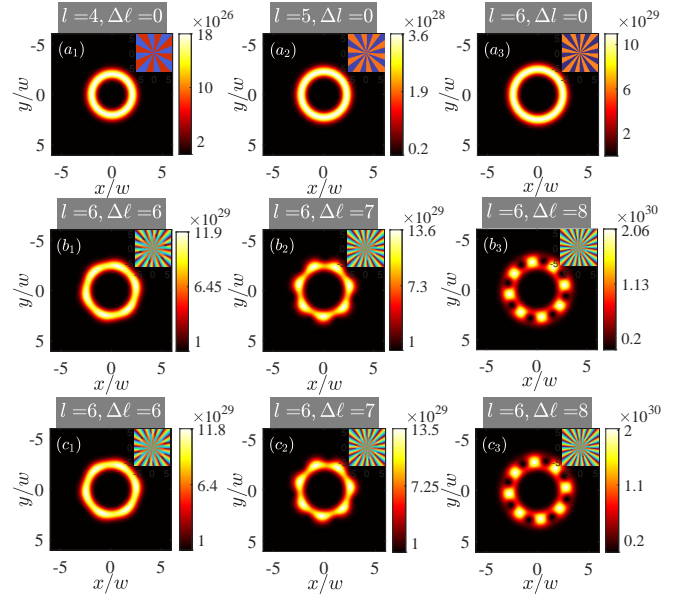


FIG. 8. The spot patterns of the total output field: Absence of OAM from the atom part ($\Delta\ell\hbar = 0$), the L-G cavity carries different OAM $l\hbar$ ($l = 4, 5$ and 6) in panel (a₁), (a₂) and (a₃), respectively. The coupling fields carry different OAM (b₁), (b₂) and (b₃) with $\delta_p = \delta_c = 0$; Panel (c₁), (c₂) and (c₃) display the cases with $\delta_c = 4 \times 2\pi$ MHz. The inside panels show the spatial distribution of the phases. The coupling strength between the atom and cavity field is set as $g' = 10^{-2} \times 2\pi$ MHz, with other parameters being the same as in Fig. 4.

B. Optical vortices in the output field

We recognize two fundamental observations regarding manipulating orbital angular momentum in our system. Firstly, a vortex cavity system enhances the input Laguerre-Gaussian beam with an extra $2l\hbar$ of OAM at the output stage. Secondly, the interaction with an atomic ensemble capable of FWM further modulates the cavity mode's OAM by an increment of $\Delta\ell\hbar$. These considerations render a discussion on the optical vortices present in the output field both pertinent and significant. The operator of the cavity field is redefined so that it carries phase information (OAM):

$$a \rightarrow \tilde{a} = \tilde{a}_s + \delta\tilde{a} = a_s e^{2il\theta} + \delta a e^{2i\ell\theta}. \quad (23)$$

Accordingly, the form of the total output field can be expressed as

$$\tilde{\mathcal{E}}_{out} = \tilde{\mathcal{E}}_{out}^s + \tilde{\mathcal{E}}_{out}^+ \mathcal{E}_p e^{-i\delta_p t} + \tilde{\mathcal{E}}_{out}^- \mathcal{E}_p e^{i\delta_p t}, \quad (24)$$

where

$$\begin{aligned} \tilde{\mathcal{E}}_{out}^s &= 2\kappa a_s e^{2il\theta} - \mathcal{E}_d, \\ \tilde{\mathcal{E}}_{out}^+ &= 2\kappa \delta a_+ e^{2i\ell\theta} - 1, \\ \tilde{\mathcal{E}}_{out}^- &= 2\kappa \delta a_- e^{2i\ell\theta}. \end{aligned} \quad (25)$$

We first consider the situation with a nonzero detuning between the driving field and the cavity mode ($\Delta_c \neq 0$). In

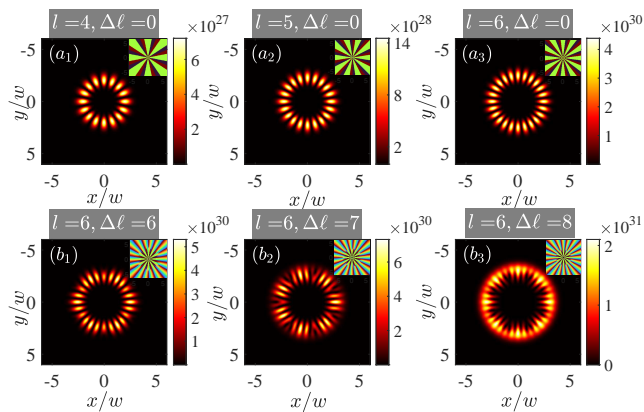


FIG. 9. The spot patterns of the total output field $\tilde{\mathcal{E}}_{out}^s$ as a function of (x, y) , with $\omega_p = \omega_d = \omega_c$. The other parameters used here are the same as in Fig. 8.

this scenario, for the probe frequency, the total output spot's complex amplitude obtained on the left side of the hybrid system should be denoted as $\mathcal{E} = \eta\mathcal{E}_p e^{-2il\theta} + \tilde{\mathcal{E}}_{out}$. Here, the first term represents the portion of the probe light reflected by the left cavity wall carrying an OAM of $-2l\hbar$ after scattering by SPP, with whose reflective rate η . The other part consists of the output cavity mode of the hybrid system. With a weak coupling strength between the atom and the cavity field ($g' = 10^{-2} \times \gamma_e$), the pattern of the output spot of the total output field is shown in Fig. 8. The diameter of the Laguerre-Gaussian beams' ring pattern increase with the augmentation of l , with $\Delta\ell$ set to 0, as depicted in Fig. 8 (a₁), (a₂), and (a₃). Given the extremely weak probe intensity, the driving field and the atomic component dominate the final output beam profile. Upon incorporating the atomic manipulation, the L-G beams' intensity pattern exhibits periodic interference rings, as illustrated in Fig. 8(b₁), (b₂), and (b₃), with the number of periods equal to $\Delta\ell$, while keeping l constant. The three bottom panels demonstrate the situation where the atomic is detuned from the cavity mode ($\delta_c \neq 0$). Apart from a slight decrease in the intensity of beams, it is almost identical to the resonant case ($\delta_c = 0$). Certainly, the phase diagrams presented in the sub-figures, ranging from Fig. 8 (a₁ⁱⁿ) to Fig. 8 (c₃ⁱⁿ), provide strong support for our conclusions.

In another scenario, when the driving field, probe field, and cavity mode are all resonant ($\Delta_c = \delta_p = 0$), the total output field should be the superposition of three components, $\mathcal{E} = \eta\mathcal{E}_p e^{-2il\theta} + \eta\mathcal{E}_d e^{-2il\theta} + \tilde{\mathcal{E}}_{out}$. Here, compared to the first scenario, there is an additional component due to the reflection of the driving field by the left SPP, denoted as $\eta\mathcal{E}_d e^{-2il\theta}$, which carries an OAM of $-2l\hbar$. The total output light intensity is shown in Fig. 9(a₁), (a₂), and (a₃), whose patterns are petal-like, and the period of the petals is $2 \times 2|l|$. The atoms contribute little to the total number of outgoing fields so that the total output field can be approximated as a superposition of two vortex beams of different intensities with OAMs of $+2l\hbar$ and $-2l\hbar$, respectively. However, with increasing the coupling strength between the atoms and the cavity field to $g' = 10^{-2} \times \gamma_e$, the vortex phase factor $\Delta\ell$ carried by the

atoms changes the pattern of the total output light intensity, as shown in Fig. 9(b₁), (b₂) and (b₃). The number of petals is still $2 \times 2|l|$, but the number of pedal periods is regulated by the atomic part $\Delta\ell$.

IV. CONCLUSION

In summary, we have investigated the steady-state optical response of a hybrid system composed of a Laguerre-Gaussian vortex cavity and atomic ensemble driven into a double- Λ model. The atomic ensemble, due to the FWM process involving three vortex beams carrying OAMs ($\hbar\ell_{\alpha,\beta,\zeta}$), is induced to have a loop phase $\varphi = \Delta\ell\theta$. Initially, we analyzed the impact of two distinct four-wave mixing (FWM) coupling schemes on the OMIT spectrum of the hybrid system. It is discovered that the net OAM ($\Delta\ell\hbar$) of the closed loops formed by the atomic FWM system can switch the system's output characteristics between absorption ($\Delta\ell = 0$) and gain ($\Delta\ell = 2$), with $\theta = \pi/2$. Correspondingly, the group delay characteristics (slow light and fast light) of the output beam from the hybrid system are also controlled and switched by $\Delta\ell\hbar$. Subsequently, we found and discussed the periodicity of the output spot under various detuning conditions between the driving frequency, cavity mode frequency, and probe frequency.

This work provides insights into the modulation of L-G optomechanical cavities and the application of OAM in hybrid quantum optical systems. Based on this composite system, it is also possible to discuss the transfer and control of OAM in the atomic system by the L-G (Laguerre-Gaussian) mode in return, in which case the L-G cavity can be regarded as a special kind of OAM source. In the passive case (without cavity driving), combining vacuum fluctuations or multiple baths with different temperatures not only makes the situation more interesting but also gives rise to novel phenomena worth exploring, such as quantum heat engines with harmonic rotation.

ACKNOWLEDGMENT

This work is supported by the Jilin Scientific and Technological Development Program (20220101009JC); Scientific Research Project of Jilin Provincial Department of Education (JJKH20241411KJ); National Natural Science Foundation of China (12104107).

Appendix A: Quantised cavity output field

Here, we analyze the steady-state output of the hybrid system from an analytical perspective. Taking an example with an obvious atomic nonlinearity (\tilde{B}_0), where $\Omega_\alpha \ll \Omega_\beta \sim \Omega_\zeta$ and $\delta_c = 0$, the correlation terms of the atomic susceptibility

can be rewritten as

$$\begin{aligned} A_0 &= \frac{ig'|\Omega_\beta|^2}{\gamma_e(|\Omega_\beta|^2 + |\Omega_\zeta|^2)}, \\ \tilde{B}_0 &= \frac{-ie^{i\Delta\ell\theta}\Omega_\alpha\Omega_\beta^*\Omega_\zeta}{\gamma_e(|\Omega_\beta|^2 + |\Omega_\zeta|^2)}. \end{aligned} \quad (\text{A1})$$

According to Eq. (16), the form of the output field becomes

$$\mathcal{E}_T = \frac{2\kappa[1 - \frac{e^{i\Delta\ell\theta}g'\Omega_\alpha\Omega_\beta^*\Omega_\zeta}{\gamma_e(|\Omega_\beta|^2 + |\Omega_\zeta|^2)}]}{\kappa - \frac{g'^2|\Omega_\beta|^2}{\gamma_e(|\Omega_\beta|^2 + |\Omega_\zeta|^2)} - i\delta_p - \frac{G^2n_c}{\gamma_\phi - i\delta_p}}, \quad (\text{A2})$$

with the effective cavity field damping coefficient

$$\kappa_{\text{eff}} = \kappa - \frac{g'^2|\Omega_\beta|^2}{\gamma_e(|\Omega_\beta|^2 + |\Omega_\zeta|^2)}. \quad (\text{A3})$$

If the output is split into $\mathcal{E}_T = u_p + iv_p$ by the real and imaginary parts, then a discussion is needed on the values of $\Delta\ell\theta$. Three distinct cases are examined for $\Delta\ell = 0, 1, 2$, under the assumption that $\theta = \pi/2$.

Taking $\Delta\ell = 0$, firstly, we can easily get $e^{i\Delta\ell\theta} = 1$. According to Eq. (A2), the real and imaginary parts of the output field can be obtained separately as

$$\begin{aligned} v_p^{\Delta\ell=0} &= \frac{2\kappa\gamma_e\delta_p\mathcal{M}\Omega^2(\gamma_e\Omega^2 - g'\Omega_\alpha\Omega_\beta^*\Omega_\zeta)}{DD}, \quad (\text{A4}) \\ u_p^{\Delta\ell=0} &= \frac{2\kappa(\gamma_e\Omega^2\mathcal{N} - g'^2\Omega_\beta^2\mathcal{G})(\gamma_e\Omega^2 - g'\Omega_\alpha\Omega_\beta^*\Omega_\zeta)}{DD}, \end{aligned}$$

where $\Omega^2 = \Omega_\beta^2 + \Omega_\zeta^2$, $\mathcal{G} = \gamma_\phi^2 + \delta_p^2$, $\mathcal{M} = G^2n_c + \delta_p^2 + \gamma_\phi^2$, $\mathcal{N} = \kappa\delta_p^2 - G^2n_c\gamma_\phi + \kappa\gamma_\phi^2$, and $DD = \gamma_e^2\Omega^4[\kappa^2\mathcal{G} + (\delta_p^2 + G^2n_c)^2 + \gamma_\phi^2\delta_p^2 - 2\gamma_\phi\kappa G^2n_c] - g'^2\Omega_\beta^2(2\gamma_e\mathcal{N}\Omega^2 - g'^2\Omega_\beta^2\mathcal{G})$.

Secondly, with $\Delta\ell = 2$ so as to $e^{i\Delta\ell\theta} = -1$, thus the real/imaginary parts of the output field will read as

$$\begin{aligned} v_p^{\Delta\ell=2} &= \frac{2\kappa\gamma_e\delta_p\mathcal{M}\Omega^2(\gamma_e\Omega^2 + g'\Omega_\alpha\Omega_\beta^*\Omega_\zeta)}{DD}, \quad (\text{A5}) \\ u_p^{\Delta\ell=2} &= \frac{2\kappa(\gamma_e\Omega^2\mathcal{N} - g'^2\Omega_\beta^2\mathcal{G})(\gamma_e\Omega^2 + g'\Omega_\alpha\Omega_\beta^*\Omega_\zeta)}{DD}. \end{aligned}$$

Similar to the above two cases, taking $\Delta\ell = 1$, we can correspondingly yield $e^{i\Delta\ell\theta} = i$, attaining those as

$$\begin{aligned} v_p^{\Delta\ell=1} &= \frac{2\kappa[\delta_p\gamma_e^2\Omega^2\mathcal{M} + g'\Omega_\alpha\Omega_\beta^*\Omega_\zeta(\gamma_e\Omega^2\mathcal{N} - g'^2\Omega_\beta^2\mathcal{G})]}{DD}, \quad (\text{A6}) \\ u_p^{\Delta\ell=1} &= \frac{2\kappa\gamma_e\Omega^2(\gamma_e\Omega^2\mathcal{N} - g'^2\Omega_\beta^2\mathcal{G} - g'\delta_p\mathcal{M}\Omega_\alpha\Omega_\beta^*\Omega_\zeta)}{DD}. \end{aligned}$$

Obviously, according to Eq. (A4) and Eq. (A5), the conversion of the vortex phase factor between 0 and 2 will change the sign of $\gamma_e\Omega^2 \mp g'\Omega_\alpha\Omega_\beta^*\Omega_\zeta$. In other words, the sign of the real and imaginary parts of the output field will be directly changed, which leads to distinct absorption/gain (v_p) phenomena.

Appendix B: The group delay of the output field

Here we will use analytic calculations to show the form of the group delay. According to the phase of the relevant output field

$$\Theta = \arg[t_p], \quad (\text{B1})$$

we can get the conversion relationship as follows

$$\frac{\partial \tan[\Theta]}{\partial \omega} = \frac{\partial \tan[\Theta]}{\partial \Theta} \cdot \frac{\partial \Theta}{\partial \omega}. \quad (\text{B2})$$

Since the group delay can be written as

$$\tau_g = \frac{\partial \Theta}{\partial \omega}, \quad (\text{B3})$$

we can simplify it by using Eq. (B2), then the group delay has the form

$$\begin{aligned} \tau_g &= \frac{\partial \Theta}{\partial \omega} = \frac{\partial \tan[\Theta]}{\partial \omega} \cdot \frac{1}{1 + \tan^2[\Theta]} \\ &= \frac{\partial \frac{v_p}{u_p - 1}}{\partial \omega} \cdot \frac{(u_p - 1)^2}{(u_p - 1)^2 + v_p^2} \end{aligned} \quad (\text{B4})$$

where

$$\tan[\Theta] = \frac{\text{Im}[t_p]}{\text{Re}[t_p]} = \frac{v_p}{u_p - 1}. \quad (\text{B5})$$

- [1] L. Allen, M. J. Padgett, and M. Babiker, *Prog. Opt.* **39**, 291 (1999).
 [2] M. Padgett, J. Courtial, and L. Allen, *Phys. Today* **57**, 35 (2004).

- [3] V. Y. Bazhenov, M. V. Vasnetsov, and M. S. Soskin, *JETP Lett.* **52**, 429 (1990).
 [4] V. Y. Bazhenov, M. S. Soskin, and M. V. Vasnetsov, *J. Mod. Opt.* **39**, 985 (1992).

- [5] A. Jesacher, A. Schwaighofer, S. Fürhapter, C. Maurer, S. Bernet, and M. Ritsch-Marte, *Opt. Express* **15**, 5801 (2007).
- [6] M. W. Beijersbergen, R. P. C. Coerwinkel, M. Kristensen, and J. P. Woerdman, *Opt. Commun.* **112**, 321 (1994).
- [7] S. S. R. Oemrawsingh, E. R. Eliel, J. P. Woerdman, E. J. K. Versteegen, J. G. Kloosterboer, and G. W. 't Hooft, *J. Opt. A* **6**, S288 (2004).
- [8] L. Marrucci, C. Manzo, and D. Paparo, *Phys. Rev. Lett.* **96**, 163905 (2006).
- [9] W. Ji, C. H. Lee, P. Chen, W. Hu, Y. Ming, L. J. Zhang, T. H. Lin, V. Chigrinov, and Y. Q. Lu, *Sci. Rep.* **6**, 25528 (2016).
- [10] P. Chen, S. J. Ge, L. L. Ma, W. Hu, V. Chigrinov, and Y. Q. Lu, *Phys. Rev. Appl.* **5**, 044009 (2016).
- [11] Z. Dutton and J. Ruostekoski, *Phys. Rev. Lett.* **93**, 193602 (2004).
- [12] J. Ruseckas, G. Juzeliūnas, P. Öhberg, and S. M. Barnett, *Phys. Rev. A* **76**, 053822 (2007).
- [13] Q. F. Chen, B. S. Shi, Y. S. Zhang, and G. C. Guo, *Phys. Rev. A* **78**, 053810 (2008).
- [14] H. R. Hamed, J. Ruseckas, and G. Juzeliūnas, *Phys. Rev. A* **98**, 013840 (2018).
- [15] H. R. Hamed, J. Ruseckas, E. Paspalakis, and G. Juzeliūnas, *Phys. Rev. A* **99**, 033812 (2019).
- [16] H. R. Hamed, E. Paspalakis, G. Žlabys, G. Juzeliūnas, and J. Ruseckas, *Phys. Rev. A* **100**, 023811 (2019).
- [17] S. H. Asadpour, E. Paspalakis, and H. R. Hamed, *Phys. Rev. A* **103**, 063705 (2021).
- [18] M. Mahdavi, Z. Amini Sabegh, M. Mohammadi, M. Mahmoudi, and H. R. Hamed, *Phys. Rev. A* **101**, 063811 (2020).
- [19] Z. P. Wang, Y. F. Zhang, E. Paspalakis, and B. L. Yu, *Phys. Rev. A* **102**, 063509 (2020).
- [20] Rahmatullah, M. Abbas, Ziauddin, and S. Qamar, *Phys. Rev. A* **101**, 023821 (2020).
- [21] S. H. Asadpour, Ziauddin, M. Abbas, and H. R. Hamed, *Phys. Rev. A* **105**, 033709 (2022).
- [22] C. Meng, T. Shui, and W. X. Yang, *Phys. Rev. A* **107**, 053712 (2023).
- [23] M. Babiker, W. L. Power, and L. Allen, *Phys. Rev. Lett.* **73**, 1239 (1994).
- [24] V. E. Lembessis and M. Babiker, *Phys. Rev. A* **82**, 051402 (2010).
- [25] D. Moretti, D. Felinto, and J. W. R. Tabosa, *Phys. Rev. A* **79**, 023825 (2009).
- [26] L. Veissier, A. Nicolas, L. Giner, D. Maxein, A. S. Sheremet, E. Giacobino, and J. Laurat, *Opt. Lett.* **38**, 712 (2013).
- [27] N. Radwell, T. W. Clark, B. Piccirillo, S. M. Barnett, and S. Franke-Arnold, *Phys. Rev. Lett.* **114**, 123603 (2015).
- [28] S. Sharma and T. N. Dey, *Phys. Rev. A* **96**, 033811 (2017).
- [29] H. R. Hamed, V. Kudriašov, J. Ruseckas, and G. Juzeliūnas, *Opt. Express* **26**, 28249 (2018).
- [30] J. E. Curtis, B. A. Koss, and D. G. Grier, *Opt. Commun.* **207**, 169 (2002).
- [31] R. Otori, T. Kobayashi, and A. Suzuki, *Opt. Lett.* **22**, 816 (1997).
- [32] S. Fürhapter, A. Jesacher, S. Bernet, and R. M. Monika, *Opt. Express* **13**, 689 (2005).
- [33] F. Tamburini, G. Anzolin, G. Umbriaco, A. Bianchini, and C. Barbieri, *Phys. Rev. Lett.* **97**, 163903 (2006).
- [34] A. Jesacher, R. M. Monika, and R. Piestun, *Optica* **2**, 210 (2015).
- [35] Z. J. Yan and N. F. Scherer, *J. Phys. Chem. Lett.* **4**, 2937 (2013).
- [36] Q. W. Zhan, *Opt. Express* **12**, 3377 (2004).
- [37] J. Wang, J. Y. Yang, I. M. Fazal, N. Ahmed, Y. Yan, H. Huang, Y. X. Ren, Y. Yue, S. Dolinar, M. Tur, *et al.*, *Nat. Photonics* **6**, 488 (2012).
- [38] A. E. Willner, H. Huang, Y. Yan, Y. Ren, N. Ahmed, G. Xie, C. Bao, L. Li, Y. Cao, Z. Zhao, J. Wang, M. P. J. Lavery, M. Tur, S. Ramachandran, A. F. Molisch, N. Ashrafi, and S. Ashrafi, *Adv. Opt. Photon.* **7**, 66 (2015).
- [39] G. Gibson, J. Courtial, M. J. Padgett, M. Vasnetsov, V. Pas'ko, S. M. Barnett, and F. A. Sonja, *Opt. Express* **12**, 5448 (2004).
- [40] J. Wang, *Photon. Res.* **4**, B14 (2016).
- [41] S. E. Harris, *Phys. Today* **50**, 36 (1997).
- [42] G. S. Agarwal and S. M. Huang, *Phys. Rev. A* **81**, 041803 (2010).
- [43] S. Weis, R. Rivière, S. Deléglise, E. Gavartin, O. Arcizet, A. Schliesser, and T. J. Kippenberg, *Science* **330**, 1520 (2010).
- [44] A. H. Safavi-Naeini, T. P. M. Alegre, J. Chan, M. Eichenfield, M. Winger, Q. Lin, J. T. Hill, D. E. Chang, and O. Painter, *Nature* **472**, 69 (2011).
- [45] B. Chen, C. Jiang, and K. D. Zhu, *Phys. Rev. A* **83**, 055803 (2011).
- [46] D. E. Chang, A. H. Safavi-Naeini, M. Hafezi, and O. Painter, *New J. Phys.* **13**, 023003 (2011).
- [47] X. G. Zhan, L. G. Si, A. S. Zheng, and X. X. Yang, *J. Phys. B* **46**, 025501 (2013).
- [48] V. Fiore, Y. Yang, M. C. Kuzyk, R. Barbour, L. Tian, and H. L. Wang, *Phys. Rev. Lett.* **107**, 133601 (2011).
- [49] F. Farman and A. R. Bahrapour, *Phys. Rev. A* **91**, 033828 (2015).
- [50] S. A. McGee, D. Meiser, C. A. Regal, K. W. Lehnert, and M. J. Holland, *Phys. Rev. A* **87**, 053818 (2013).
- [51] K. N. Qu and G. S. Agarwal, *Phys. Rev. A* **87**, 031802 (2013).
- [52] X. B. Yan, C. L. Cui, K. H. Gu, X. D. Tian, C. B. Fu, and J. H. Wu, *Opt. Express* **22**, 4886 (2014).
- [53] M. Bhattacharya and P. Meystre, *Phys. Rev. Lett.* **99**, 153603 (2007).
- [54] M. Bhattacharya, P. L. Giscard, and P. Meystre, *Phys. Rev. A* **77**, 030303 (2008).
- [55] Z. Chen, J. X. Peng, J. J. Fu, and X. L. Feng, *Opt. Express* **27**, 29479 (2019).
- [56] F. Wang, K. Shen, and J. Xu, *New J. Phys.* **24**, 123044 (2023).
- [57] S. M. Huang, L. Deng, and A. X. Chen, *Ann. Phys.* **534**, 2200171 (2022).
- [58] Y. M. Liu, C. H. Bai, D. Y. Wang, T. Wang, M. H. Zheng, H. F. Wang, A. D. Zhu, and S. Zhang, *Opt. Express* **26**, 6143 (2018).
- [59] J. X. Peng, Z. Chen, Q. Z. Yuan, and X. L. Feng, *Phys. Rev. A* **99**, 043817 (2019).
- [60] J. X. Peng, Z. Chen, Q. Z. Yuan, and X. L. Feng, *Phys. Lett. A* **384**, 126153 (2020).
- [61] Z. C. Zhang, J. C. Pei, Y. P. Wang, and X. G. Wang, *Front. Phys.* **16**, 1 (2021).
- [62] Y. Xu and W. J. Liu, *J. Lightwave Technol.* **41**, 2246 (2022).
- [63] E. X. DeJesus and C. Kaufman, *Phys. Rev. A* **35**, 5288 (1987).
- [64] K. G. Makris, R. El-Ganainy, D. N. Christodoulides, and Z. H. Musslimani, *Phys. Rev. Lett.* **100**, 103904 (2008).
- [65] S. Klaiman, U. Günther, and N. Moiseyev, *Phys. Rev. Lett.* **101**, 080402 (2008).
- [66] C. Hang, G. X. Huang, and V. V. Konotop, *Phys. Rev. Lett.* **110**, 083604 (2013).
- [67] J. T. Sheng, M.-A. Miri, D. N. Christodoulides, and M. Xiao, *Phys. Rev. A* **88**, 041803 (2013).
- [68] D. Huo, S. Hua, X. D. Tian, and Y. M. Liu, *Opt. Express* **31**, 16251 (2023).
- [69] L. Ge and H. E. Türeci, *Phys. Rev. A* **88**, 053810 (2013).

- [70] J. H. Wu, M. Artoni, and G. C. La Rocca, Phys. Rev. Lett. **113**, 123004 (2014).
- [71] J. H. Wu, M. Artoni, and G. C. La Rocca, Phys. Rev. A **91**, 033811 (2015).
- [72] F. Yang, Y. C. Liu, and L. You, Phys. Rev. A **96**, 053845 (2017).
- [73] P. W. Milonni, *Fast light, slow light and left-handed light* (CRC Press, 2004).
- [74] F. Badshah, M. L. Murtza, S. Asghar, and Ziauddin, Phys. Scr. **98**, 095105 (2023).